UNIVERSITY OF CALIFORNIA,
IRVINE

Stress Analysis and Structural Diagnosis of Solid Rocket Motors using the Finite Element Method

THESIS

submitted in partial satisfaction of the requirements
for the degree of

MASTER OF SCIENCE

in Civil & Environmental Engineering

by

Marquis Anthony Mark

Thesis Committee:
Professor Lizhi Sun, Chair
Associate Professor Mo Li
Assistant Professor M.J. Abdolhosseini Qomi

2020

DEDICATION

This thesis is proudly dedicated to

My amazing family; Juataun, Hubert, Jaidyn, and Jaycee Mark
Who inspired me to be the man I am today

And

My supportive friends and partner who kept me sane through the trials and tribulations of higher education

TABLE OF CONTENTS

LIST OF FIGURES

LIST OF TABLES

ACKNOWLEDGEMENTS

First and foremost, I would like to offer my appreciation to my advisor, Dr. Lizhi Sun, for the opportunity to grow as a scholar and researcher. When I applied to UC Irvine, I originally planned on enrolling as a master's student, but Dr. Sun graciously offered me the opportunity to join his research team as a doctoral student. This has been a truly transformative experience and I appreciate all that he has done for me.

I would also like to extend my appreciation to Dr. Timothy Miller and the Airforce Research Laboratory at Edwards Air Force Base, CA for financially supporting my research efforts. AFRL researcher Dr. Timothy Miller has also supported me by sharing his vast knowledge and providing guidance when I reached roadblocks in my research. The Edwards AFRL research team also showed a great deal of hospitality when me and Dr. Sun visited for a research meeting.

Thank you to UC Irvine's graduate division, who awarded me the Diversity Recruitment Fellowship upon acceptance to UCI. This allowed me to participate in the Competitive Edge summer research program that prepared me for my experience as a PhD student.

I must also extend my gratitude to the great staff and faculty of the Civil and Environmental Engineering department. To the brilliant Dr. Mohammad Javad Abdolhosseini Qomi, who provides a unique perspective when I need professional, personal and research advice. To the amazing Dr. Mo Li, who is one of the most insightful educators I have had the privilege to study under.

Lastly and most importantly, I would like to thank my family and friends who have supported me through the many challenges that brought me to where I am today.

ABSTRACT OF THE THESIS

Stress Analysis and Structural Diagnosis of Solid Rocket Motors Using Finite Element Method

by

Marquis Anthony Mark

Master of Science in Civil & Environmental Engineering

University of California, Irvine, 2021

Professor Lizhi Sun, Chair

Stress analysis of Solid Rocket Motors (SRMs) using the finite element method provides insightful data that can be used to develop a structural diagnosis methodology. Finite element models with and without flaws were designed and subjected to thermal loads to simulate post-production storage cooling of SRMs. The models are designed with dimensions and material properties provided by researchers from the Air Force Research Laboratory (AFRL) at Edwards Air Force Base, CA. It was concluded that during the simulated cooling process, flaws create unique stress signatures dependent on flaw type, size, and location. These trends were then validated and contextualized using fracture and damage mechanic concepts. Existing methodologies for health diagnosis of SRMs are discussed and their limitations addressed. Specifically, limitations of a two-dimensional sensor-based methodology developed by AFRL and UC Irvine collaborators are critiqued for improvement. It is then proposed that a three-dimensional finite element analysis of SRMs with flaws produces more viable data for an improved health diagnosis method. In the future, results from the three-dimensional finite element analysis will serve as the basis for a new methodology supported by multi-sensor arrays and machine learning algorithms for a holistic health prognosis and diagnosis of SRMs.

1. Introduction

Structural health monitoring (SHM) is the process of assessing the health and safety of structural components and is most popularly applied to civil infrastructure. SHM has interdisciplinary applications and is predicated on research fields and concepts such as fracture and damage mechanics, multi-scale materials modeling, and the finite element method. My goal is to develop a multi-disciplinary SHM methodology that establishes a health diagnosis of solid rocket motors (SRMs) capable of detecting the presence of flaws such as bore cracks and delaminations. SRMs are typically stored for extended periods of time increasing the risk of defect nucleation and propagation. Detection of these defects is of importance because it can reduce fleet maintenance cost, prevent the disposal of healthy rockets, and even save lives.

1.1 History of Solid Rocket Motors

SRMs have played a huge role in shaping the development of human civilizations for hundreds of years. Though it is easy to first think about the complex aerospace applications we use them for in contemporary society, SRMs are relatively simple with few moving parts. In fact, the first known use of SRMs appeared in 14th century China for military applications and consisted of a cylindrical tube filled with gunpowder and a fuse. These primitive rockets were known as “fire arrows” and were used to propel large arrows over vast distances at opposing forces. Over time, SRMs have been developed for advanced military use and eventually space exploration. However, their fundamental design has changed very little.

1.2 SRM Components and their Functions

A SRM consist of three major components: the casing, insulation, and solid propellant. The purpose of the case is to contain the energy being generated during the ignition of the solid propellant. This allows the energy being generated to be directed in one direction (through a nozzle), allowing the rocket to generate significant thrust. Large amounts of energy are generated from this process so the casing must be able to sustain high temperatures and pressure. Because of this, SRM casings are designed as cylindrical thin walled pressure vessels. Materials for the casing vary from cardboard for hobby rockets to steel alloys for military and aerospace grade rockets.

The insulation serves as a layer of protection for the casing, primarily mitigating the conduction of heat from the solid propellant during operation. Insulation has several auxiliary functions as well, including facilitating the transfer of moisture and chemicals between the case and propellant, enclosing joints and fittings preventing a loss in pressure during operation, and maintaining structural integrity of the components during stretching and contraction due to temperature change [1]. The importance of these auxiliary functions become clear when developing newer and more complex SRMs leading to much proprietary research being done to design unique insulative materials.

The bulk of an SRM is the solid propellant, a material with a high energy density used to generate large amounts of thrust when ignited. Contemporary SRMs make use of composite propellants, consisting of several chemical components such as fuel, binders, oxidizers and curing agents. The most common and consistently used solid propellant is ammonium perchlorate (AP) based composite propellants that where developed and

heavily researched in the 1960s and 1970s [1]. These propellants are so reliable they are still commonplace to this day. Though the general design of SRMs has remained relatively unchanged, the complexity of their use has facilitated the development of new materials.

1.3 Common SRM Flaws

Large sums of money, capital and lives are invested into SRMs so it is key to understand typical flaws and subsequent failure modes that may occur. Every component of a SRM is susceptible to developing flaws but the leading cause of SRM failures are due to the nozzle and propellant [2]. The scope of this research focuses on solid propellant and its interaction with other components due to its unique properties and multitude of failure types. Common defects and flaws associated with the solid propellant is aging effects, bore cracks and delaminations between the insulation and propellant.

SRM fleets can be placed in storage for years or even decades prior to being used resulting in an aging effect within the solid propellant. During this idle time, solid propellant can undergo changes due to physical, chemical, and mechanical processes. These processes included chemical decomposition via hydrolysis, softening due to cyclic temperature changes, and diffusion of moisture from the propellant to the insulation [3]. This leads to significant changes to the solid propellant's mechanical properties and material responses. These changes cause unpredictable effects on the SRMs operational capacity rendering them unusable.

Bore cracks in solid propellant is quite common and are believed to nucleate during the cooling process SRMs undergo after curing. There is a general consensus that small bore cracks that are a few percent of the grain thickness are no reason for concern.

Moreover, determining what signifies a critical crack size is quite nuanced and still not entirely agreed upon [4]. Nonetheless, there are warranted efforts to understand their nucleation and propagation in hopes of detecting them prior to operation of an SRM. Existing bore cracks can propagate during operation causing an increase and concentration of pressure ultimately resulting in case rupture [5].

SRMs experience a variety of temperature changes causing the components to expand and contract leading to the nucleation of delaminations. Delaminations occurs when materials that are designed to be bonded begin to separate. These delaminations can occur between the propellant, insulation, and the casing but the presented research focuses on debonding between the propellant and insulation. This can result in similar operational hazards as bore cracks such as concentrated pressures and temperatures in undesirable locations. My research shows each flaw type causes unique stress patterns and understanding these patterns is key to the effectively diagnosing SRMs.

1.4 Benefits of SRM Health Diagnosis

The ability to effectively and efficiently monitoring the health of a SRM fleet is beneficial for several reasons. For one, solid rocket motors are used in conjunction with human operated orbiters such as the space shuttle endeavor that have carried over 350 astronauts over the course of 135 missions [6]. Thus, failure of a solid rocket booster due to inadequate health diagnosis can lead to the tragic loss of lives. Additionally, an effective health diagnosis can significantly reduce cost associated with a fleet of SRMs. It can prevent the disposal of healthy rockets if one representative SRM is deemed inoperable from a rudimentary diagnostic technique. Also, SRM fleets include redundant rockets due to the

uncertainty of their health over time. An accurate health diagnosis technique would allow manufactures to comfortably reduce the number of supplementary SRMs for such logistical reasons.

1.5 Existing Diagnosis Methodologies

Developing a methodology to detect the presence of flaws in aerospace components and even SRMs is not a novel idea. Flaw detection techniques vary and there has been special interest in developing non-destructive evaluation (NDE) techniques, especially for costly aerospace structures. NDE allows for the detection of flaw while ensuring the structural component remains operable. Examples include use of advanced diagnostic imaging (X-Ray, CT, MRI, etc.), sensor technology and visual inspection. An interesting example is the use of non-evasive piezo-electric sensors to monitor structural integrity of aluminum structures such as aircraft wings [7]. This utilization of the electromechanical impedance method is quite popular in the field of structural health monitoring.

It is arguable that use of sensor technology is the most appealing method to develop a SHM process for SRMs. Visual inspections are subject to human error and advanced diagnostic imaging is not applicable to larger SRMs. Sensors are ideal for monitoring SRMs due to their reliability and longevity considering a rocket needs to be continuously monitored for decades possibly. There have been several research efforts exploring the use of sensors and sensors design specifically for health monitoring of SRMs. Chelner and Buswell proved that specially designed embedded dual-bond stress-temperature (DBST) sensors can be used to facilitate estimates of SRMs service life and detect the presence of flaws [8]. Further research efforts have eventually shown the same DBST sensors can

estimate the size and location of bore cracks and delaminations using a simplified 2D elastic approach [9] [10]. This research was done by research collaborators at the Air Force Research Laboratory (AFRL) at Edwards Air Force Base, CA based on a similar finite element stress analysis process. However, the methodology only included stress analysis from two-dimensional models. The finite element models used were also based on simplified approaches to modeling flaws such as bore cracks and delaminations.

Use of fiber optic sensor technology is another interesting way to monitor the health of SRMs. Riziotis et al argue photonic sensors such as polymer optical fibers (POFs) are the preferable solution for continuous structural health monitoring of solid propellant in SRMs [11] [12]. The researchers showed POFs can be embedded in solid propellant and provide accurate strain readings during a SRMs lifetime including operation. POFs can be as small as 650nm and have a inherit immunity to electromagnetic interference making them a versatile and reliable sensor technology. However, there are a few limitations regarding its application as a structural health monitoring tool. First, the process requires excellent bonding between the propellent and the casing of the fiber. If this is not achieved, slippage could occur ultimately effecting the strain readings from the POF. Additionally, under high strains the polymers fibers undergo plastic deformation ultimately effecting their strain readings. Lastly, the POFs capability of estimating defect types and sizes is not explored, it is simply acknowledged that abnormal strain readings are indicative of a defect.

More recently, researchers developed a piezoelectric sensor-based health monitoring technique to detect delaminations at the propellant-insulation interface [13]. The method was developed by conducting piezoelectric electromechanical impedance

testing in finite element modeling software. A piezoelectric sensor is attached to a structure and subjected to an alternating electric field inducing small deformations in the sensor. This can be used to predict defects by comparing the small deformations, or electromechanical impedance spectra, of damaged and undamaged specimen. Xiao et al concluded that a piezoelectric sensor can be placed on the outside of an SRM casing to monitor debonding conditions and detect delaminations if they occur. Though the research provided promising results, it does have limitations as well. Piezoelectric sensors are only sensitive to local debonding conditions, so the health monitoring technique requires many sensors or more advance sensors with an extended sensing region. Additionally, the methodology is limited to detecting delaminations and has not been applied to detecting other flaws such as bore cracks to my knowledge.

2. Methodology

To develop a holistic structural diagnosis of SRMs, one must first understand the conditions and stresses that persist in a rocket motor through its service life. To start, SRMs are manufactured by pouring propellant in a liquid form in a cast consisting of the case and insulation. Once poured, the propellant begins to cure until it is eventually solid. In this solid state, the propellant is at a stress-free cure temperature and begins to cool until it reaches ambient storage temperate. The following stress analysis simulates the post-cure cooling process until ambient temperature is reached. The cooling process is simulated with commercially available finite element software ABAQUS. During and after this process radial stresses persist in the solid propellant and stress analysis shows this is radially constant in SRMs without flaws. However, gradual ambient cooling can cause stress perturbations from existing or developing flaws to disturb this constant radial stress.

The goal of this research is to qualitatively and quantitively characterize the relationship between radial stress perturbations, flaw type, and flaw size to develop a structural health monitoring methodology for SRMs. Details of how this simulation is structured and executed is as follows.

2.1 Model Dimensions

Sizes and shapes of SRMs vary greatly based on their service and functionality. For example, the propellants Web Fraction (WF) is directly responsible for the burn time and rate of the rocket [14]. It is a function of the solid propellant's inner diameter and outer diameter as shown in Equation 2.1. Analysis of SRMs with different web fractions has shown they have unique internal stresses but overall patterns from flaw-induced stress perturbations are similar. This implies this methodology can be applied to SRMs of various Web Fraction values. Additionally, the bore hole of a SRM can take many forms from star shaped to anchor shaped based on its function. For my analysis I modeled a simple circular bore hole. Investigation on effects of bore shape was not conducted. Dimensions used for this simulation were provided by collaborators from the Air Force Research Laboratory (AFRL) at Edwards Air Force Base, CA. The model includes the SRM three basic components: the case, insulation, and solid propellant. Casing was modeled at 3.175mm thick and insulation at 2.54mm thick. The solid propellant has an inner diameter (I.D) of 203.2mm and outer diameter (0.D) of 406.4mm (Figure 2.1). For three-dimensional analysis, the same plan dimension is used, and the motor was assumed to be a midsection of an SRM and modeled with a depth 250mm.

Equation 2.1 – Web Fraction Formula

$$WF = \frac{Propellant\ O.D - Propellant\ I.D}{Propellant\ O.D} \quad (2.1)$$

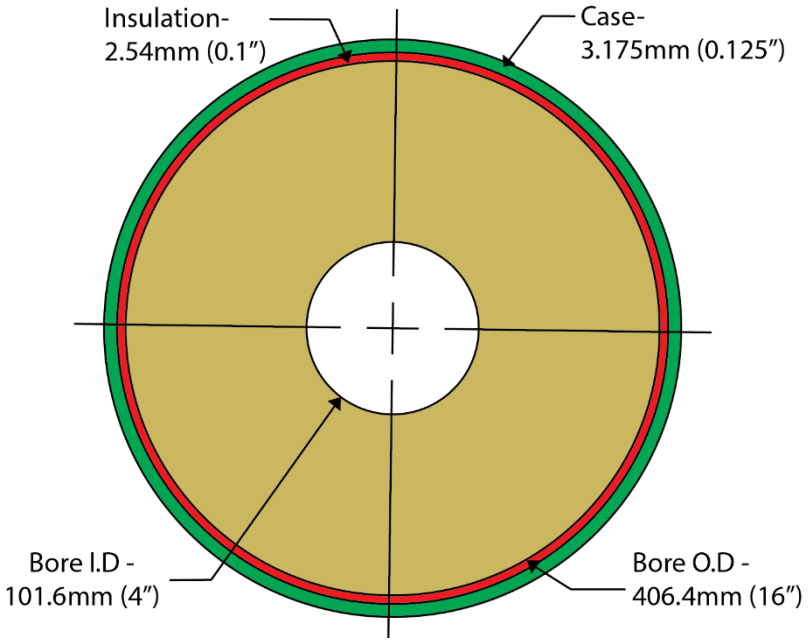

Figure 2.1 – Plan view of solid rocket motor dimensions for 2D and 3D analysis

2.2 Defining Loading Conditions

As noted, the model simulates the SRM cooling from a cure temperature of 58°C to storage temperature at -40°C. An additional 2°C temperature drop is added to the cure temperature to account for cure shrinkage effects, indicating a total temperature drop of 100°C [9]. It is assumed the SRM cools gradually so the temperature load is simulated in a quasi-static fashion with 10°C increments. This is important to note because it effects how the material responses are defined in the model for my analysis as discussed in Chapter 2.3.

2.3 Defining Material Properties

For my analysis, a filament-wound graphite-epoxy motor (GEM) is used for the casing and modeled with quasi-isotropic thermal-elastic responses [15]. An ethylene

propylene diene monomer (EPDM) liner is used for the insulation. The solid propellant is modeled as typical composite grain of hydroxyl-terminated polybutadiene (HTPB) matrix with an ammonium perchlorate (AP) oxidizer. Both the insulation and solid propellant material properties were obtained from in-house testing at the Edwards Air Force Base AFRL. A simplified thermal-elastic response is used for both as well. Mechanical properties of the EPDM case and AP/HTPB solid propellant can be seen in Table 2.1 and 2.2. Insulation mechanical properties are excluded due to its proprietary nature. It is worth noting that solid propellant is a composite, and a nonlinear viscoelastic material response would be a more accurate representation of the material. However, because thermal loading is assumed to be long term and quasi-static, a thermal-elastic material response is sufficient for preliminary analysis. This will be discussed in further detail in Chapters 3 and 4.

Table 2.1 – Casing mechanical properties

Filament-Wound GEM Case		
Young's Modulus (MPa)	**Poisson's Ratio**	**Coefficient of Thermal Expansion**
55,900	0.3	2.16E-06

2.4 Determining Proper Boundary Conditions

For the simulation to yield reliable results, boundary conditions applied to the SRM should closely resemble real world scenarios. To determine this, I considered how SRMs are typically placed sideways in storage. This is true for small-scale and large-scale rockets alike and can be seen in Figure 2.2. As shown, the SRM is straddled by half-circle shaped supports that prevent lateral movement and rotation is assumed to be prevented due to friction. Based on this, the boundary condition can be idealized into a simple pinned connection (Figure 2.3).

Table 2.2 – Solid propellant mechanical properties

HTPB/AP Propellant			
Temperature (°C)	**Young's Modulus (MPa)**	**Poisson's Ration**	**Coefficient of Thermal Expansion**
-40	32.128	0.499	9.558E-5
-34	28.219	0.499	9.558E-5
-29	24.785	0.499	9.558E-5
-23	21.794	0.499	9.558E-5
-18	19.212	0.499	9.558E-5
-12	17.007	0.499	9.558E-5
-7	15.144	0.499	9.558E-5
-1	13.592	0.499	9.558E-5
4	12.316	0.499	9.558E-5
10	11.284	0.499	9.558E-5
16	10.463	0.499	9.558E-5
21	9.819	0.499	9.558E-5
27	9.32	0.499	9.558E-5
32	8.933	0.499	9.558E-5
38	8.623	0.499	9.558E-5
43	8.359	0.499	9.558E-5
49	8.107	0.499	9.558E-5
54	7.834	0.499	9.558E-5
60	7.507	0.499	9.558E-5

Figure 2.2 – Solid rocket motor in storage [26]

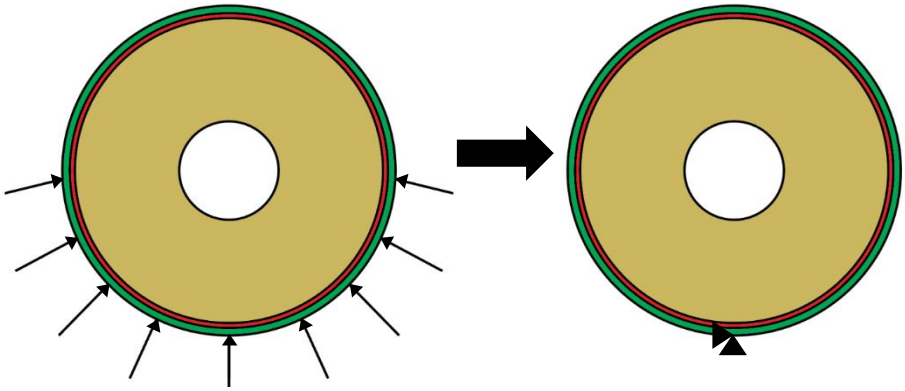

Figure 2.3 – Derivation of idealized boundary conditions

2.5 Mesh Design and Element Selection

Careful consideration was put into the design of the mesh and types of elements used for both the two-dimensional and three-dimensional SRM analysis**.** For the two-dimensional finite element analysis, modified plane-strain second-order quadrilateral elements were used. Second-order elements (8-Node) were used as opposed to first-order (4-node) because of their superior ability to capture stress singularities, an expected phenomenon for bore cracks and delaminations. For three-dimensional finite element analysis, modified 3D stress first-order (8-Node) hexahedron elements were used. Though use of second-order (20-Node) elements would undoubtedly be more accurate, their associated computational loads exceed current capabilities. To compensate for this, flaw regions where heavily meshed with fine elements. For both two-dimensional and three-dimensional analysis, the propellant has a Poisson ratio of 0.499 so hybrid element modification was applied. This introduces pressure as an independent variable preventing computational problems with nearly incompressible materials such as solid propellant. The elements were further modified to utilize reduced-order integration to minimize computation times. It is assumed this is permissible due to the fine nature of the mesh implemented in the models.

2.6 – Mesh Independence Investigation

A mesh independence investigation was conducted to ensure the mesh geometry, element size and element quantity had little to no effect on my results. This also ensures accurate results while minimizing the computational load required to run the large number of simulations required for the proposed methodology. It was found that mesh symmetry effected results so an average global element size of 7.5mm is used to maintain this

requirement for both 2D and 3D models. It is most important to ensure the mesh is fine enough near the flaws to fully capture the associated stress singularities. To do so, multiple variations of two-dimensional SRM Models with a bore crack or delamination flaw where modeled and simulated. For each flaw, three variations were modeled with varying element sizes categorized as course, fine or very fine. Collected data from each scenario and subsequent variations can be seen in Table 2.3. Though the "fine" element size was found to be sufficient for two-dimensional analysis, "very fine" element sizes were used for the three-dimensional analysis for reasons discussed in Chapter 2.5.

Table 2.3 – Mesh independence investigation for element size near flaws

Comparison of 2D Models with Different Finite Element Meshes				
	Mesh Description	Course	Fine	Very Fine
Bore Crack (25.4mm)	Avg. Element Size at Flaw (mm)	0.5	0.1	0.01
	Max Radial Stress at insulation-grain interface (MPa)	2.93	3.05	3.10
	Min. Radial Stress at insulation-grain interface (MPa)	2.91	2.85	2.80
Delamination (15 Degrees)	Avg. Element Size at Flaw (mm)	0.25	0.05	0.01
	Max Radial Stress at insulation-grain interface (MPa)	12.2	12.6	12.7
	Min. Radial Stress at insulation-grain interface (MPa)	-0.75	-0.65	-0.62

3. Two-Dimensional Analysis Results & Discussion

3.1 – Background to Experiment

For the 2-Dimensional analysis, two common flaws that occur in solid propellant are considered: bore cracks and delamination's. SRMs are typically designed with stress-relieving slots near both ends of the propellant. So, it is assumed flaws have the tendency to initiate at the mid-plane of the motor and propagate longitudinally [9]. With this, it can be

inferred that a 2-Dimensional plain-strain analysis can be used to investigate how such flaws effect stresses within the propellant. This is illustrated in Figure 3.1a and 3.1b. Section A-A of each figure is the location the two-dimensional models in relation to an SRM. Dimensions of these models are shown in Figure 2.1.

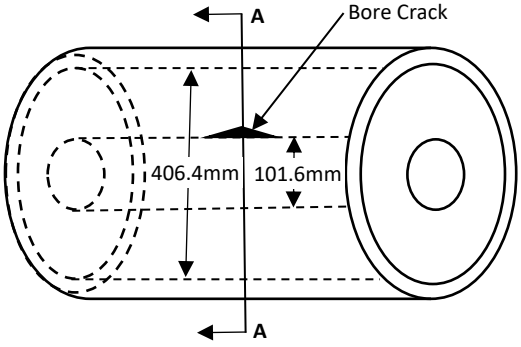

Figure 3.1a – Schematic of a SRM midsection with a bore crack at mid-span

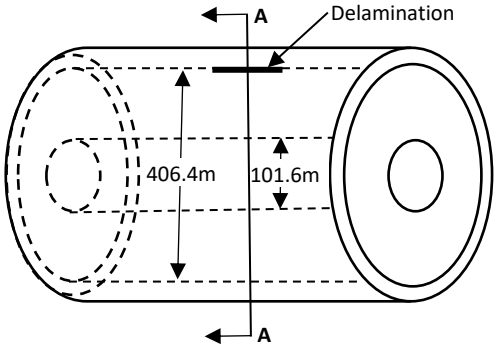

Figure 3.1b – Schematic of a SRM midsection with a delamination at mid-span

First, it is key to understand stress patterns in a SRM without a flaw to serve as a baseline or control for my data. To do so, SRMs where modeled without flaws and subjected to loading conditions as defined in Chapter 2.2. Results show stresses are radially constant throughout the propellant. This is illustrated by the constant circular bands of stress in the radial stress contour plot shown in Figure 3.2a. Figure 3.2b shows this is true at the propellant-insulation interface as well and illustrated in the radial stress contour plot of isolated section at this interface (Note: elements shown in the figures are part of the whole model but are displayed isolated solely for illustrative purposes). This is also numerically shown and further discussed in Chapter 3.2 and 3.3. The radial stress value at the propellant-insulation interface of a SRM without a flaw will serve as a baseline when comparing the effects of stress perturbation from flaws moving forward. This is done because DBST sensors can be placed at the propellant-insulation and measure

radial stress at certain intervals. By collecting and analyzing stress data for various bore crack and delamination sizes from FEM models, flaw-dependent patterns can be cataloged. These patterns will serve as the basis of my SRM health prognosis methodology.

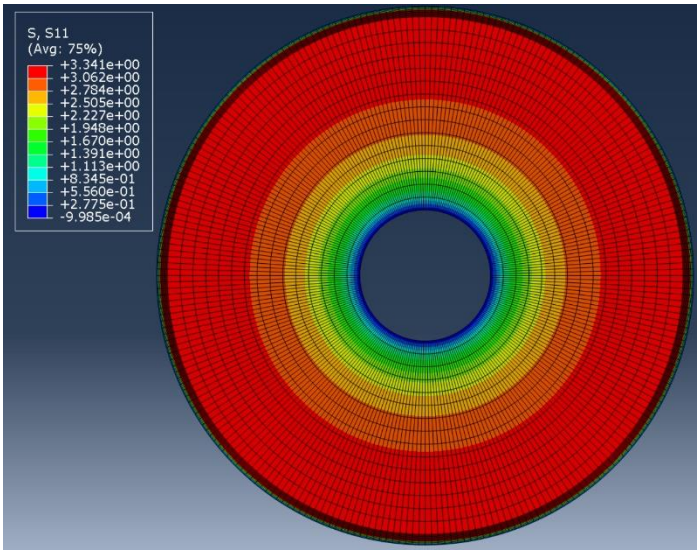

Figure 3.2a – Radial stress contour plot of a SRM without a flaw introduced

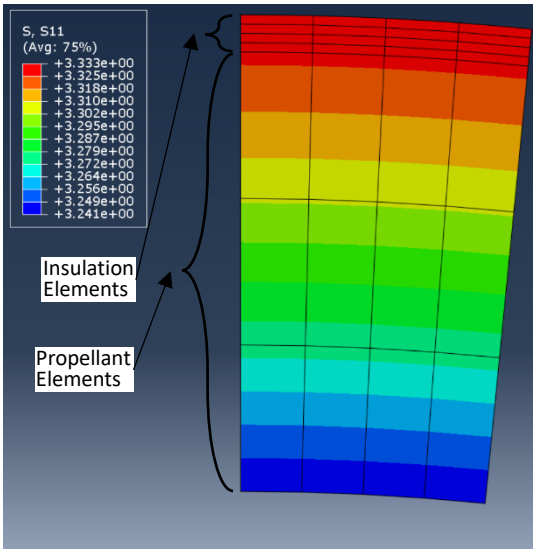

Figure 3.2b – Radial stress contour plot of isolated elements at the propellant-insulation interface

3.2 Bore Crack Analysis and Results

The first step of my bore crack analysis was understanding the shape of the crack itself. For initial analysis, a point crack was used. Later, the composite nature of solid propellant was considered. Solid propellant is composed of a matrix with embedded solid grain particles, so it can be assumed that aggregate bridging occurs. This results in a "real crack" and "fictitious crack" where particles bridge between the crack face (Figure 3.3). With this in mind, I determined that a notch-shape crack would be more appropriate for my analysis and ran simulations for both crack shapes. A comparison of their geometries

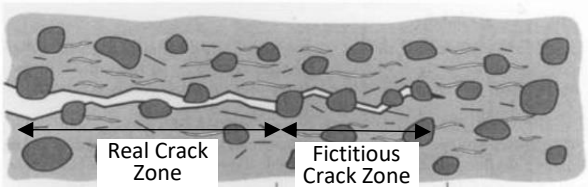

Figure 3.3 – Crack with aggregate bridging resulting in a real crack zone and fictitious crack zone [24] (Modified)

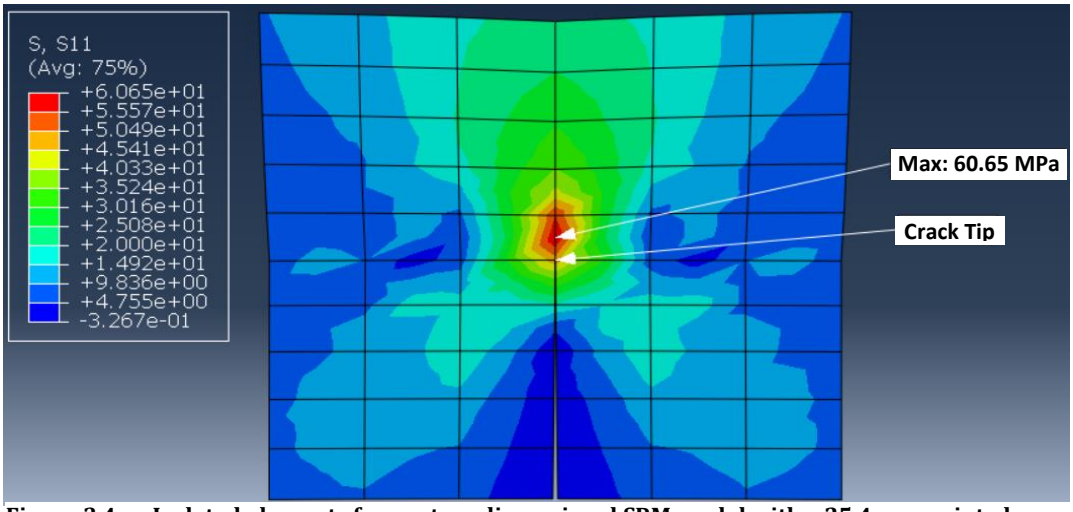

Figure 3.4a – Isolated elements from a two-dimensional SRM model with a 25.4 mm point-shape crack

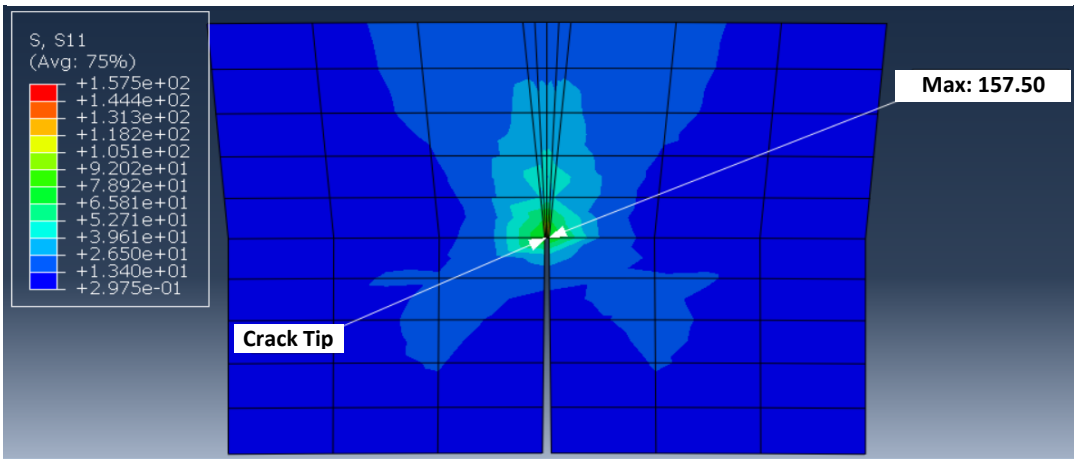

Figure 3.4b – Isolated elements from a two-dimensional SRM model with a 25.4mm notch-shape crack

and stress singularity values at the crack tips can be seen in Figure 3.4a and 3.4b. As shown, the notch-shape crack has a stress singularity value more than 1.5x that of the point crack. Radial stress was measured along the propellant-insulation interface for each crack type to further investigate their differences. It was found that radial stress at the interface for each model was completely identical indicating the crack shape has no discernible effect on my two-dimensional bore crack analysis.

To develop an understanding of stress perturbations due to bore cracks, a total of 5 bore crack sizes where modeled and simulated. Radial stress was measured along the

propellant-insulation interface starting from an angular position of 0° above the bore crack to 360° around the circumference of the interface. This is illustrated in Figure 3.5 and resulting plots for each crack size can be seen in Figure 3.6 and 3.7. As shown, each bore crack effected the radial stress at the interface similarly by causing a reduction of radial stress when compared to the baseline no flaw value. The larger the crack, the more this radial stress reduction is. Additionally, remnants of the crack tips stress singularity can be seen at an angular position of 0° where there is a local peak in radial stress. This is followed by a gradual dip in stress until another local peak at 180° from the crack tip. It is worth noting that the local peak in stress at 180° is greater than the one at 0° above the crack tip.

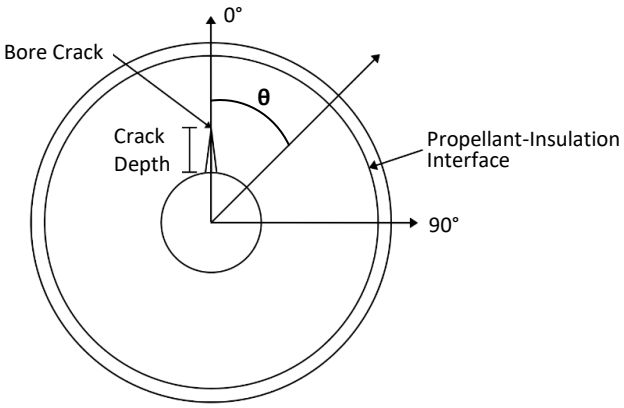

Figure 3.5 – Schematic illustrating how SRMs with bore cracks are modeled and parameters for data collection

It is also worth noting how a SRMs Web Fraction effects the results from the bore crack analysis. Figure 3.8 shows two different SRMs with a Web Fraction of 0.50 and 0.75, respectively. Similar simulations were conducted on the former and radial stress plots for various bore crack sizes can be seen in Figure 3.7. The model with a WF of 0.50 has a baseline stress of 0.85MPa while the SRM with a WF of 0.75 has a baseline stress of 3.33 MPa. Additionally, bore cracks in the model with a WF of 0.50 had a more drastic effect on the stresses at the interface. More specifically, the stresses at an angular position of 0° above the bore crack at the interface often exceed the baseline value of 0.85MPa.

Nonetheless, the patterns are quite similar for each model; a reduction in radial stress at the interface with a peak in stress at an angular position of 0° and 180° from the crack tip.

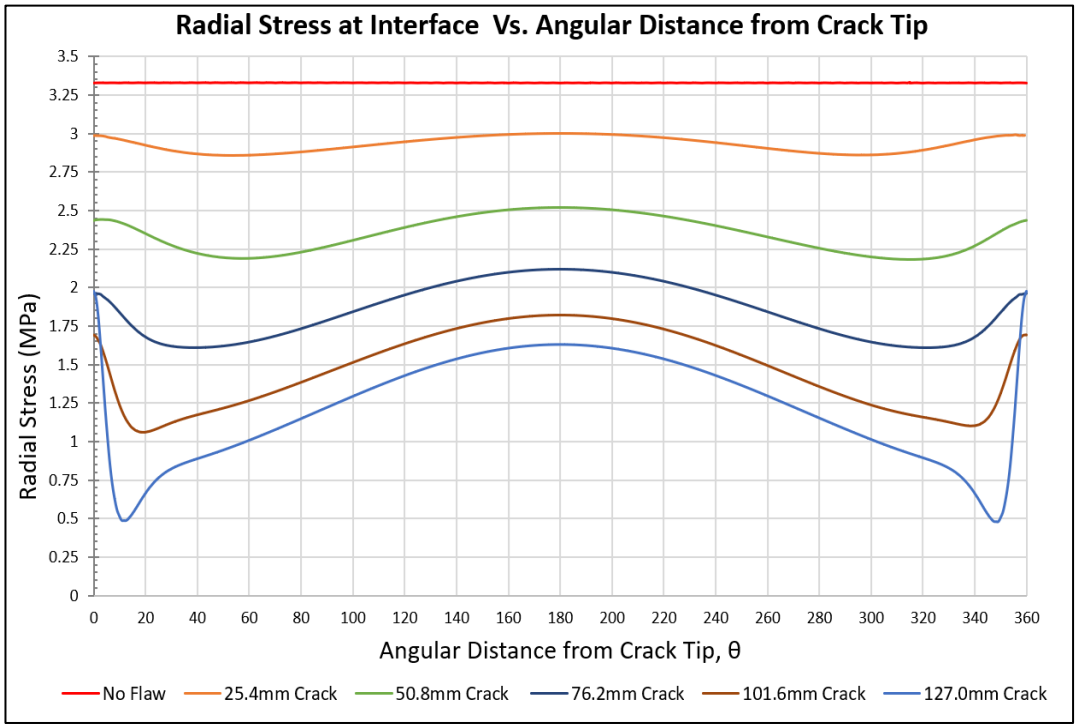

Figure 3.6 - Radial stress along propellant-insulation interface for various bore crack sizes on SRM with WF of 0.75

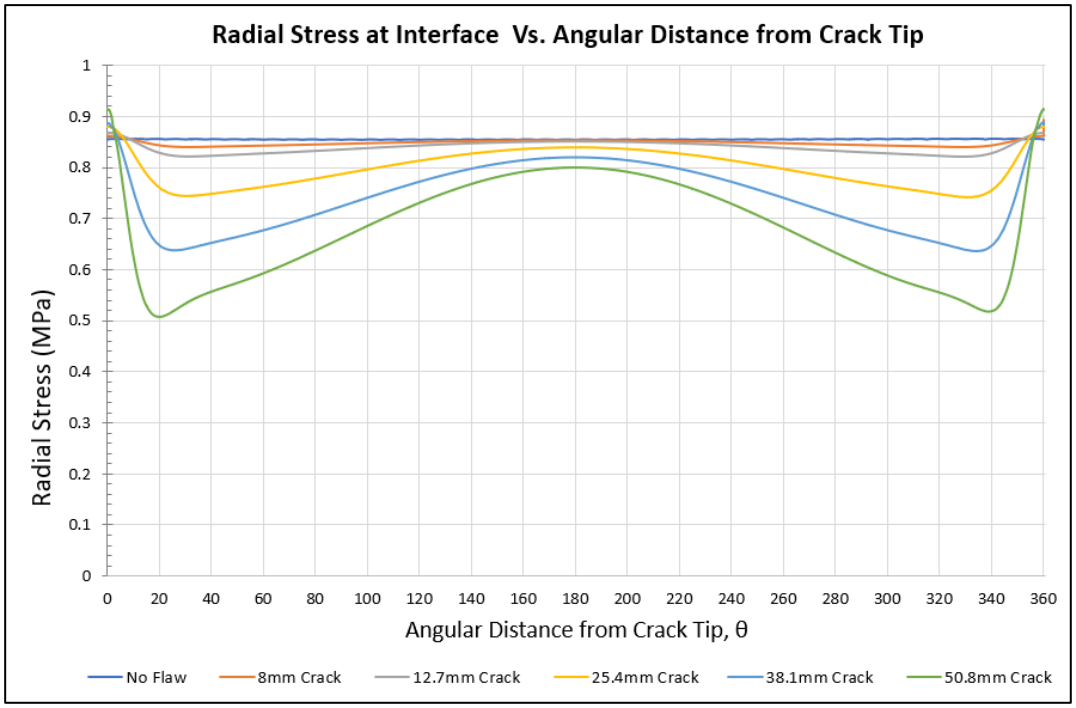

Figure 3.7 - Radial stress along propellant-insulation interface for various bore crack sizes for on SRM with a WF of 0.50

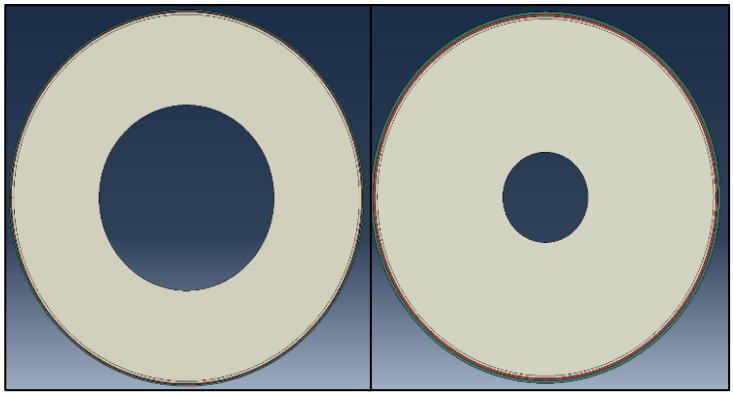

Figure 3.8 – 2D SRM models with a WF of 0.50 (Left) and WF of 0.75 (Right)

3.3 - Delamination Analysis and Results

Data from the delamination flaws were obtained similarly to the bore crack. The primary difference is how the flaw was modeled. Instead of removing material from the propellant in the shape of a flaw like the bore crack, a seam was introduced to the insulation grain interface to simulate the presence of a delamination. This creates two layers of nodes at the interface allowing the grain and insulation to separate as the SRM deforms due to the temperature load. To ensure the simulation captures the stress singularity at each flaw tip (two for the case of the delamination), a refined mesh is used at their locations. A visualization of the mesh near the flaw before and after deformation can be seen below in Figure 3.9.

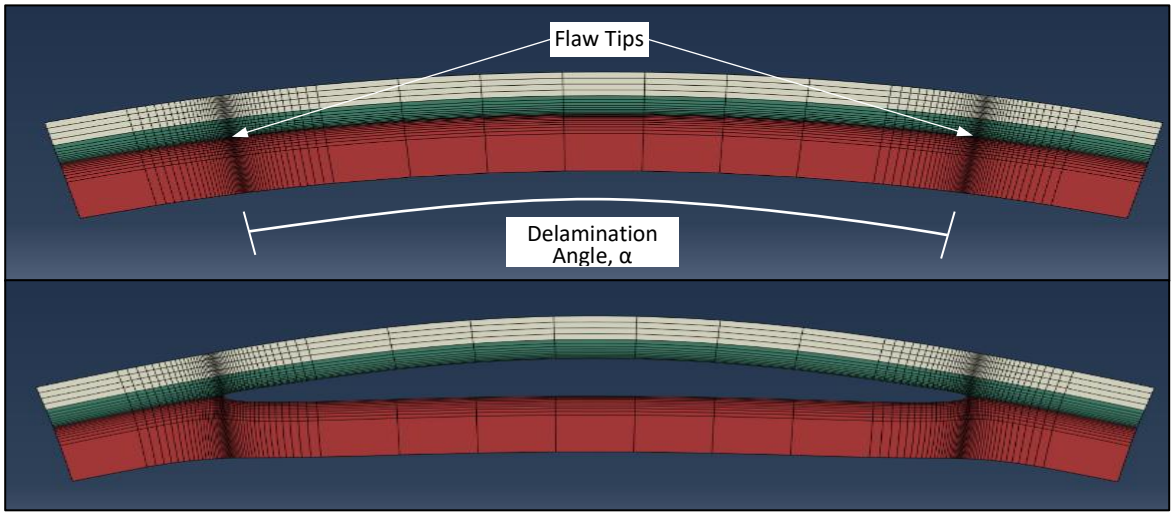

Figure 3.9 – Isolated elements at the delamination before deformation (top) and after (bottom)

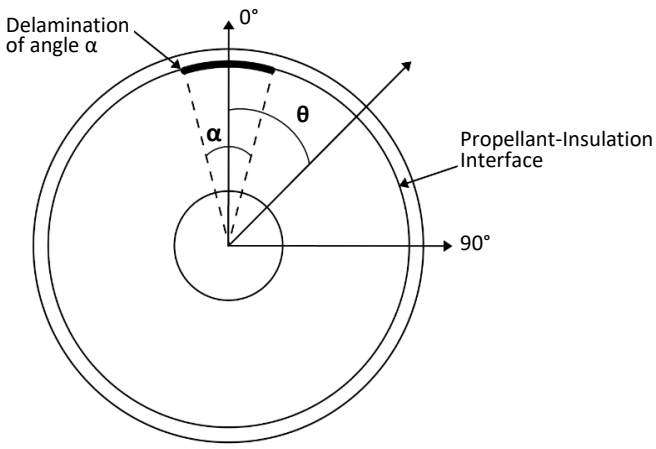

Figure 3.10 - Schematic illustrating how SRMs with delaminations are modeled and parameters for data collection

A total of 4 delamination sizes where modeled designated by delamination angles α. A visualization of these debond angles and the corresponding radial stress plots are presented in Figure 3.10 and Figure 3.11, respectively. The radial stress plots show there is a large stress singularity near each tip of the delamination while stress is 0 along the flaw interface. This is followed by a sharp dip in stress and a reduction in radial stress at the insulation-propellant interface when compared to the no flaw baseline model.

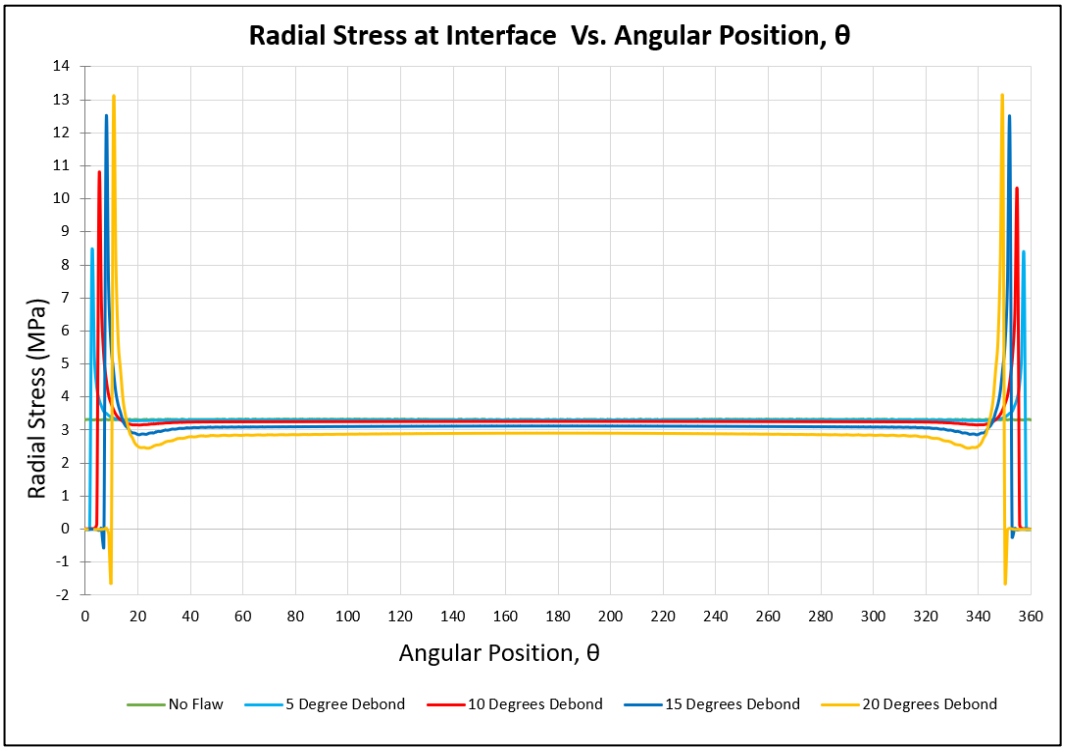

Figure 3.11 - Radial stress along propellant-insulation interface for various delamination angles

3.4 Multiple Flaw Scenario Analysis Results

To ensure the proposed SRM health prognosis and diagnosis methodology is holistic, it must be capable of identifying the likely scenario that multiple flaws are present. Such scenarios would undoubtedly cause different stress perturbation patterns than those of a single flaw scenario. However, collecting enough data to quantitively and qualitatively characterize these patterns would require an inextricably large number of scenarios be modeled and simulated. To mitigate this, the superposition method is employed to create multiple-flaw scenarios data sets without running the associated simulation. Superposition principles applies to stress fields if linear elasticity is assumed, allowing for the combination of stress fields from various models [17]. Figure 3.12 illustrates how stress fields from multiple scenarios can be combined to emulate the stress field of a single scenario.

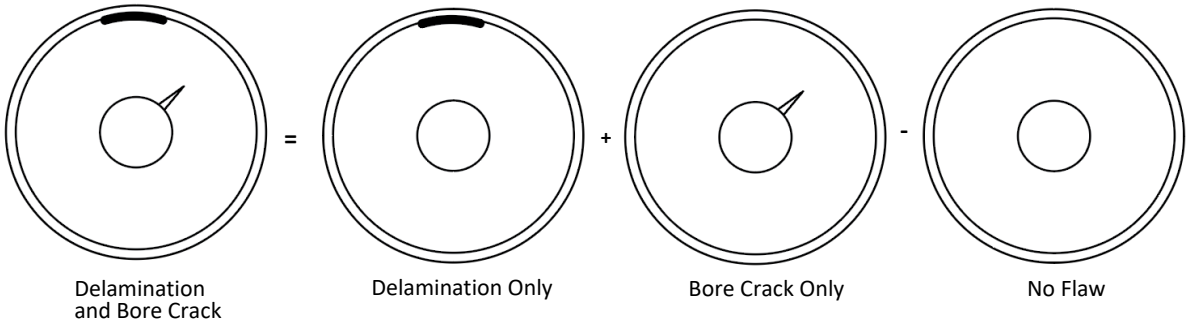

Figure 3.12 – Use of superposition method to estimate stress fields

To validate this superposition method, multi-defect scenarios were modeled which included the presence of a bore crack and a delamination at various angular distances from each other. One such example can be seen in Figure 3.13 where a 50.8mm bore crack and 15° delamination are spaced 45° from each other. These scenarios were simulated under the same loading conditions to generate radial stress plots like the ones presented in Chapters 3.3 and 3.5. The same radial stress data was estimated using the superposition

method mentioned prior and then compared to the data from the finite element models. Results from the two-dimensional stress analysis of the model seen in Figure 3.13 are shown in Figure 3.14. As seen, the data sets are nearly comparable indicating the superposition method is viable for my analysis.

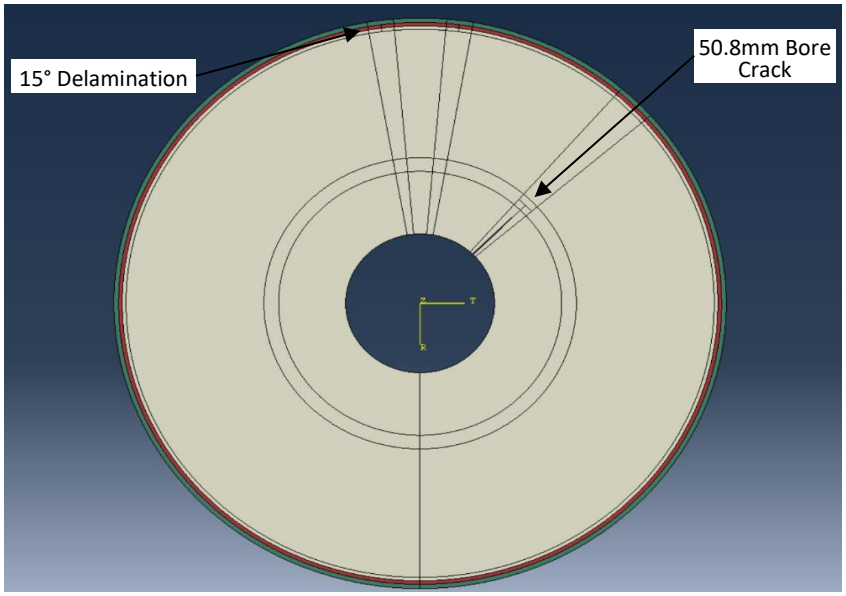

Figure 3.13 – 2D SRM model with a 50.8mm bore crack and 15° delamination spaced 45° from each other

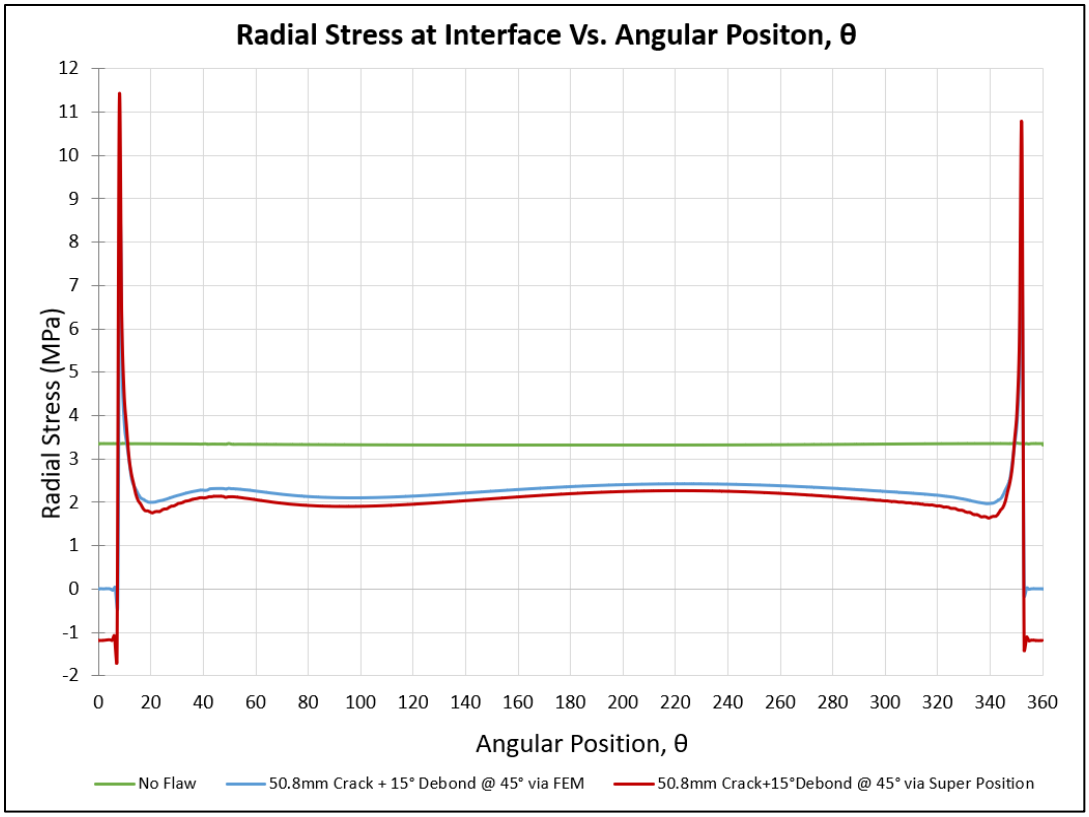

Figure 3.14 – Radial stress plots comparing data from a multi-flaw finite element model (FEM) and data derived from the super position method

3.5 Two-Dimensional Stress Analysis Discussion

As seen in the results, different flaws of various sizes leave unique stress signatures in SRMs during their cooling process. Bore cracks reduce radial stress throughout the propellant with two local peaks. Delaminations result in high stress singularities at the delamination tips and cause smaller reductions in radial stress compared to bore cracks. It was also shown that the combination of bore cracks and a delamination produce another unique stress signature, one that can be predicted using the superposition method. Knowledge of physics behind flaw phenomenon can provide context and further our understanding of the trends displayed in Chapter 2. Furthermore, such understanding ensures that an efficient and accurate diagnosis technique for SRMs is developed. Though

the preliminary two-dimensional results are insightful, limitations can be found in the experiments design.

3.5.1 – Contextualizing Results with Fracture Mechanic Concepts

Given the simple approach to the problem at hand, basic concepts of Linear Elastic Fracture Mechanics (LEFM) can explain much of the trends seen in the bore crack and delamination results. The most notable is the idea of a stress singularity at the flaw tip where infinite stress exist, an idea proposed by the pioneer of fracture mechanics George Rankin Irwin [18]. Irwin defined a new fundamental concept knows as the stress intensity factor which describes the severity of stresses at the crack tip. A visualization of this concept is seen in Figure 3.4 where stresses at the crack tip are much larger than the surrounding area. Remnants of this stress singularity are visible in both the bore crack and delamination results in Figure 3.6 and 3.11 validating the observed trend. This is especially evident in the delamination results where radial stress readings are taken at the crack tip itself where a large spike in stress in seen.

Another applicable fracture mechanics concept is the understanding of crack nucleation and growth due to thermal-mechanical loading. Aerospace structures such as SRMs are subjected to a multitude of mechanical and thermal loads so knowledge of this concept is key for health diagnosis. Researchers have determined that a stress intensity factor can be composed of an independent thermal stress intensity factor and mechanical stress intensity factor [19]. Furthermore, it is typical for both the mechanical and thermal load to induce compressive loads at a flaw's free edges and tensile loads near the flaw tip. Again, this is observable in Figure 3.4 and 3.11 where negative stresses are seen near the

flaws free ends and positive stress at the flaw tip, further validating the trends seen in the results.

3.5.2 Two-Dimensional Stress Analysis Results and SRM Health Diagnosis

The provided two-dimensional results can be used to develop a simple sensor-based health diagnosis of SRMs. This was proven in research efforts by Le at al where similar finite element stress analysis data was compared to sensor manufacturer data to verify if such sensors could detect flaws in SRMs [9] [10]. They concluded that placing 3-6 sensors along the insulation-grain interface and comparing their readings can indicate the presence of a flaw and even estimate its size. This is predicated by trends seen in Figure 3.6, 3.7, and 3.11. If no flaw is present in an SRM, each sensor will have the same radial stress reading as seen in the constant "No Flaw" plots. If a flaw is present, the sensors will begin to display different readings indicating the presence of a flaw. Moreover, by comparing the difference in the radial stress readings from each sensor, the flaw size can be estimated to a certain degree and dependent on the number of sensors used.

Though this novel method proved to be valid, it has its limitations. The sensors design for this methodology have an accuracy of ±10 kPa effectively bottlenecking the methods flaw size detectability. This is especially true for delaminations, considering the much smaller reductions in radial stress induced as shown in Figure 3.11. Additionally, the possibility of multiple flaws being present is not considered. This may be justified by the unlikeliness of two flaws occurring on the same plane in this two-dimensional analysis. However, it must be acknowledged that stresses and strains from the flaws exist both in plane and in the z-direction. Lastly, there is no discussion in the methods ability to predict flaw location.

3.5.3 Limitations to Two-Dimensional Stress Analysis

As stated, the preliminary two-dimensional analysis provided insightful data but has its limitations and requires further critique regarding its validity. Most notably, the two-dimensional bore crack model presented in Chapter 3.2 is more representable of a through crack than an interior crack illustrated in Figure 3.1. Meaning that the models represent a crack that spans the entire depth of the section. This was verified with three-dimensional through crack models and will be illustrated and discussed further in Chapter 4. Knowing this, it can be assumed that the sensor bases SRM diagnosis outlined in Section 3.5.2 may only be valid for bore cracks and delaminations of significant depth, justifying the plain-strain analysis approach.

In addition to this, more accurate material descriptions exist for solid propellant. AP/HTPB solid propellant is a nonlinear viscoelastic and its mechanical behavior is highly dependent on temperature, strain, and strain rate [19]. Because of this, much research is conducted with the goal of developing a constitutive model capable of accurately describing the material response. However, solid propellant experience various stresses and strains from aging effects, cyclic temperature loading and evolving microstructural damage making it very difficult design such a constitutive model. To address this, Tunç and Özüpek designed a thermo-viscoelastic constitutive model supported by a continuum damage model that could predict AP/HTPB solid propellant material responses with reasonable accuracy [21]. Nonetheless, temperature changes the SRM experiences in the described analysis is slow, suggesting only long-term elastic modulus matters, which of course varies with temperature. Therefore, a thermal-elastic response is assumed for two-

dimensional analysis. However, this may not be sufficient for three-dimensional analysis and will further discussed in Chapter 4 and later explored in future work.

Lastly, implementation of known fracture mechanics phenomena is missing from the preliminary two-dimensional analysis. One such example is the presence of a plastic zone at the crack tip. A stress singularity of infinite stress is not physically possible, so it is assumed that plastic energy dissipation occurs at the crack tip and yield stress dramatically decreases (Figure 3.15). Note this dramatic decrease in stress is observable in the delamination results illustrated in Figure 3.11 validating the observed trends. The plastic zone can take various shapes dependent on the crack size, its location, and the material itself. Determining the shape and size of the plastic zone for the solid propellant is nuanced and beyond the scope of this work. Nonetheless, reducing the elastic modulus in a region near the flaw tip, a few percent the size of the flaw itself, would be a simple way to represent a plastic zone for my analysis [23].

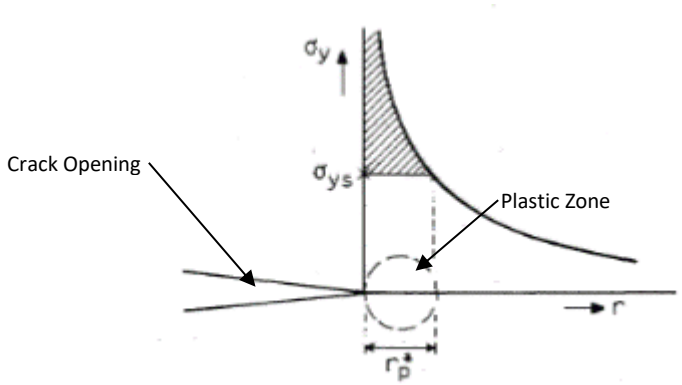

Figure 3.15 – Illustration of a stress singularity and plastic zone at a crack tip [22]

4. Three-Dimensional Analysis Results and Discussion

To further understanding of flaw induced stress patterns, the next logical step is to expand stress analysis to a three-dimensional model. Stresses from flaws persist outside of the perspective planes illustrated in the two-dimensional analysis. The goal of the three-dimensional analysis is to determine how and to what degree do these stresses propagate longitudinally. Only delaminations are considered in the three-dimensional analysis and stress effects from bore cracks are currently under investigation. Ultimately, insight on three-dimensional flaw induced stress patterns will lend itself to a more accurate structural diagnostic method for SRMs.

4.1 – Background to Experiment

The three-dimensional SRM models are designed and simulated similarly to the two-dimensional models. A thermal load from 60°C to -40°C is applied to every node in the model to simulate ambient cooling after post-cure temperature is reached. Again, the temperature drop is modeled in a quasi-static fashion of 10°C increments to simulate gradual cooling. The same thermal-elastic material response parameters presented in Table 2.1 and 2.3 are maintained in the preliminary analysis for each material. However, future models will include implementation of a user-defined nonlinear viscoelastic constitutive model for the solid propellant. Possible benefits of this and how it may affect the results will be discussed in Section 4.3. The three-dimensional models use the plan dimensions illustrated in Figure 2.1 and are 250mm in length. The model can be seen below in Figure 4.1.

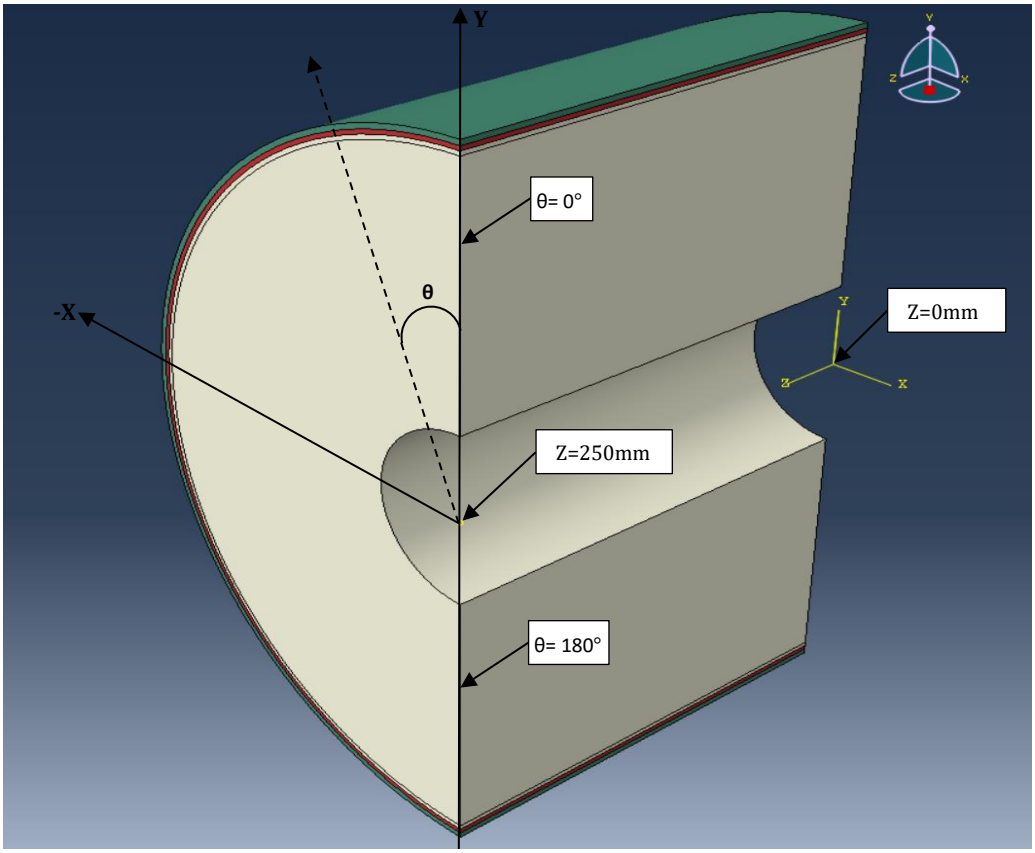

Figure 4.1 – Isometric view of three-dimensional SRM finite element model

Expanding the analysis to three dimensional requires further assumptions for proper boundary condition application. Because the large three-dimensional models are computationally taxing, they are designed to take advantage of symmetry conditions. As seen in Figure 4.1, a half-model of an SRM is considered with symmetry boundary conditions applied to the Y-Z plane. As for the faces on the Y-X plane, only displacement along the z-direction is bounded considering the model represents a midsection of an SRM. Like the two-dimensional model, there are pinned connections at the base of the model to simulate the straddling effect of typical storage conditions as discussed in Chapter 2.

Before stress analysis of three-dimensional flaws is conducted, it is key to first understand stress patterns in an undamaged SRM to serve as a baseline. Analysis shows

plane stresses are radially constant, consistent with what is seen in the two-dimensional baseline analysis. Radial stress is also constant longitudinally in the three-dimensional SRM models, a key pattern for flaw induced stress analysis. For flaw-induced stress analysis, radial stresses were measured radially at the propellant-insulation from 0° to 180°. This measurement was taken at locations of interest and 25mm intervals along the length of the SRM away from the flaw tip.

4.2 – Delamination Analysis and Results

Three-dimensional delaminations are modeled as "seams" similar to the two-dimensional analysis but there are additional considerations and assumptions required for analysis. Again, the "seam" creates two layers of nodes at the delamination interface, allowing the solid propellant and insulation to separate as the SRM deforms due to the thermal load (Figure 4.3). As for the dimensions of the delaminations, length in the z-direction requires assumptions regarding their propagation behavior. It is assumed the delamination has no preference in the direction it propagates, thus it is of equal size in both directions. For example, a 10° delamination has an arc length of 35mm at the propellant-insulation interface, so it is modeled to have a longitudinal length of 35mm (Figure 4.2). Additionally, the delaminations are located on the symmetry plane to take computational advantage of symmetry conditions. This allows for modeling of half of the delamination. For example, a 10° delamination is represented by a half-angle 5° delamination at the symmetry plane as seen in Figure 4.2.

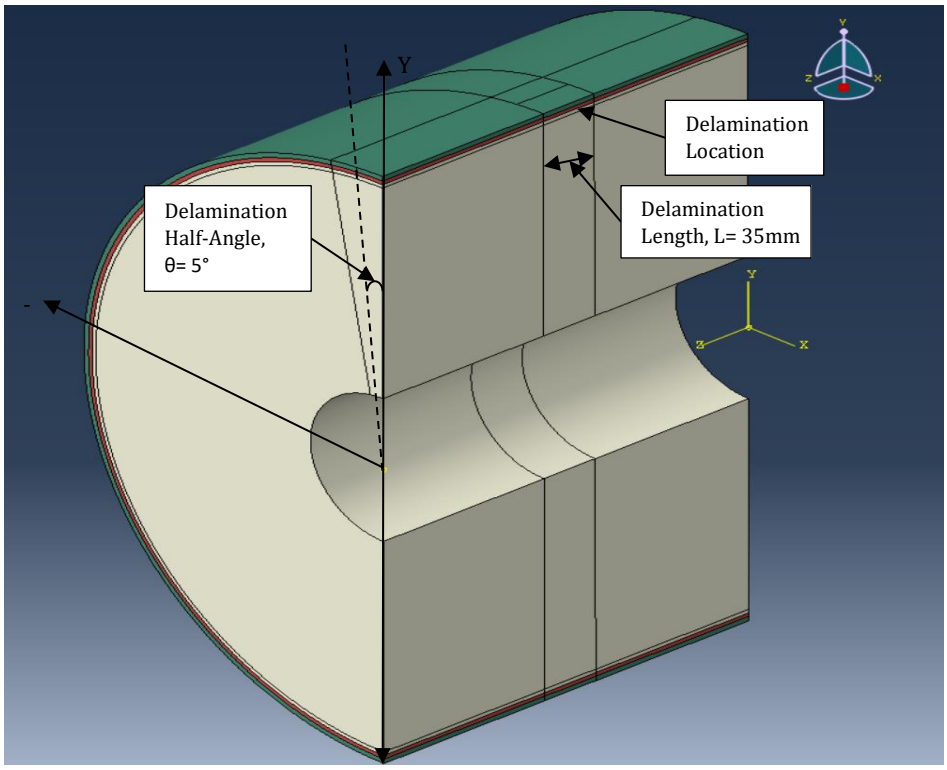

Figure 4.2 – Isometric view of three-dimensional SRM finite element model with a 10° Delamination at the symmetry plane. Delamination center is located at midspan of the model (Z=125)

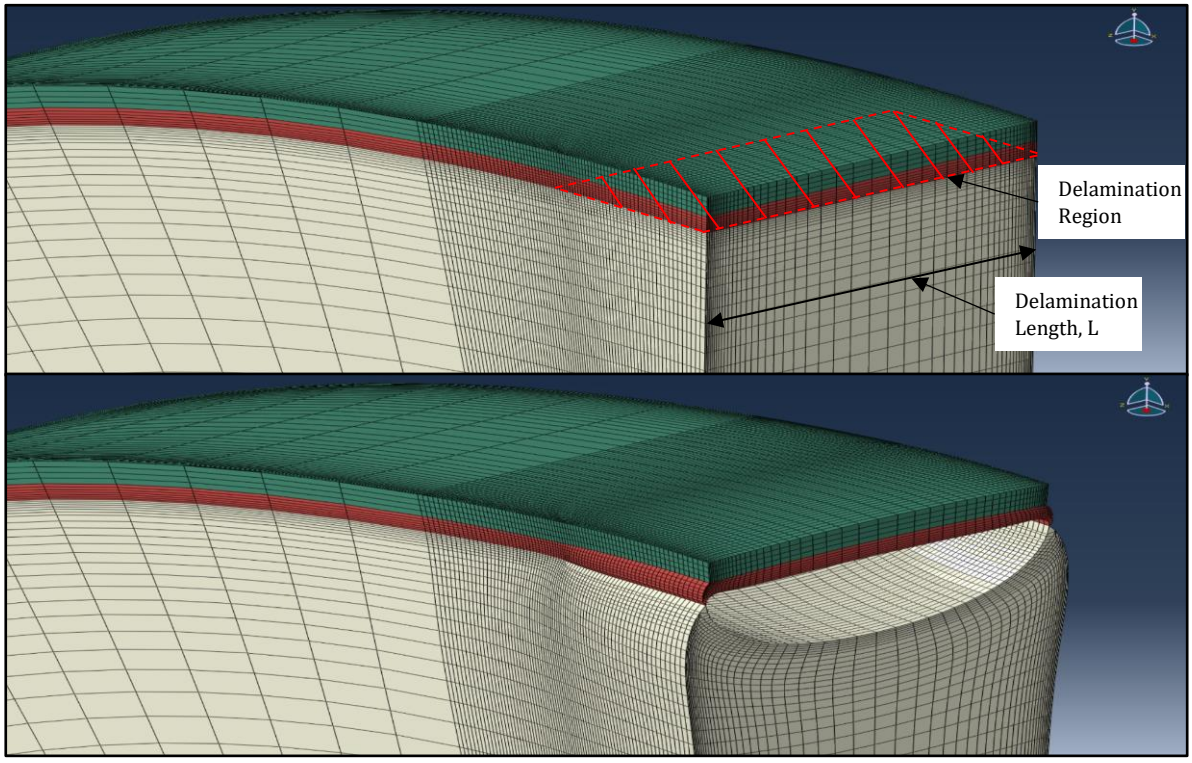

Figure 4.3 – Isolated elements at the delamination before (top) and after (bottom) deformation

Results from a 10° delamination stress analysis simulation can be seen in Figure 4.4a-b. Radial stress was measured at the propellant-insulation interface from 0° to 180° at different cross-sections along the length of the SRM model. Each cross-section is indicated by its location along the Z-axis. The first notable trend is what is seen at the delamination center line which is located at the midspan of the model (Z=125mm). There is zero radial stress at the delamination interface but as you move radially towards the flaw tip (θ=5°), there is large spike in stress (12.2 MPa), indicative of a stress singularity. The peak is followed by a steep reduction in stress until a constant radial stress is reached. This is the same trend observed in the two-dimensional 10° delamination radial stress plot in Figure 3.11.

More importantly, the three-dimensional stress analysis provided insightful information missing from the two-dimensional analysis. First, radial stress is measured in the same plane as the delamination tip (X-Y Plane) at Z=107.5mm. Here we see high radial stress values across the flaw tip from 0° to 5° followed by a steep reduction in stress. It is interesting to note how quickly the radial stress approaches a value close to a no-flaw baseline value at both the delamination center line (Z=125 mm) and tip (Z= 107.5mm). This is also reflected in the radial stress curves at 25mm intervals away from the delamination. Furthermore, Figure 4.4a suggest remnants of the stress concentration from the delamination tips are only observable approximately 10mm away from the flaw tip (see the Z=100mm curve).

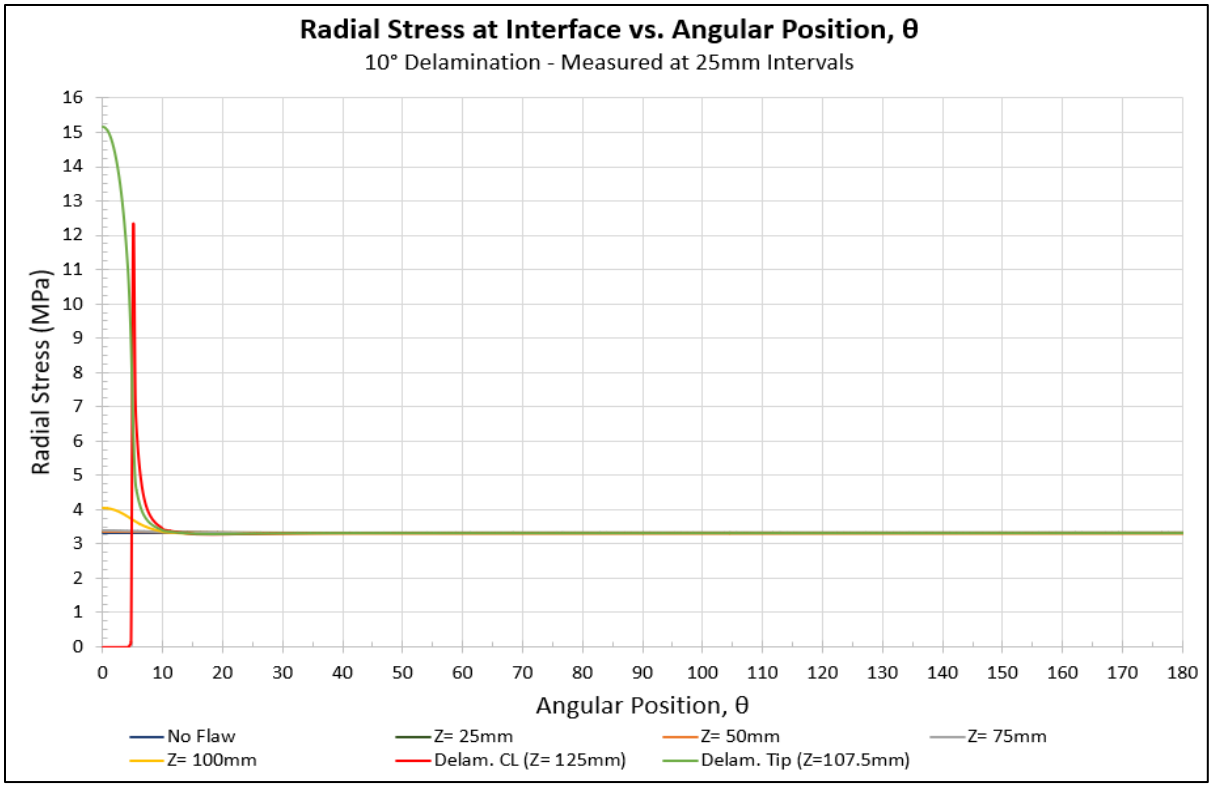

Figure 4.4a – Radial stress along propellant-insulation interface for 10° Delamination measured at 25mm intervals and locations of interest

However, Figure 4.4b provides a closer inspection at what is occurring at the propellant-insulation interface away from the delamination (note the changed Y-axis values). As seen, stress perturbations from the delamination exist at the interface as far as 80mm from the flaw. These perturbations are quite small when compared to stresses at the delamination location. For example, approximately 60mm from the delamination tip at Z= 50mm, radial stress peaks at 3.36 MPa, a 0.03 MPa increase from the no flaw baseline value of 3.33 MPa. As we move away from the delamination, this perturbation becomes smaller and smaller. It is also worth noting that a slight decrease in radial stress is seen as well, a trend also observed in the two-dimensional stress analysis.

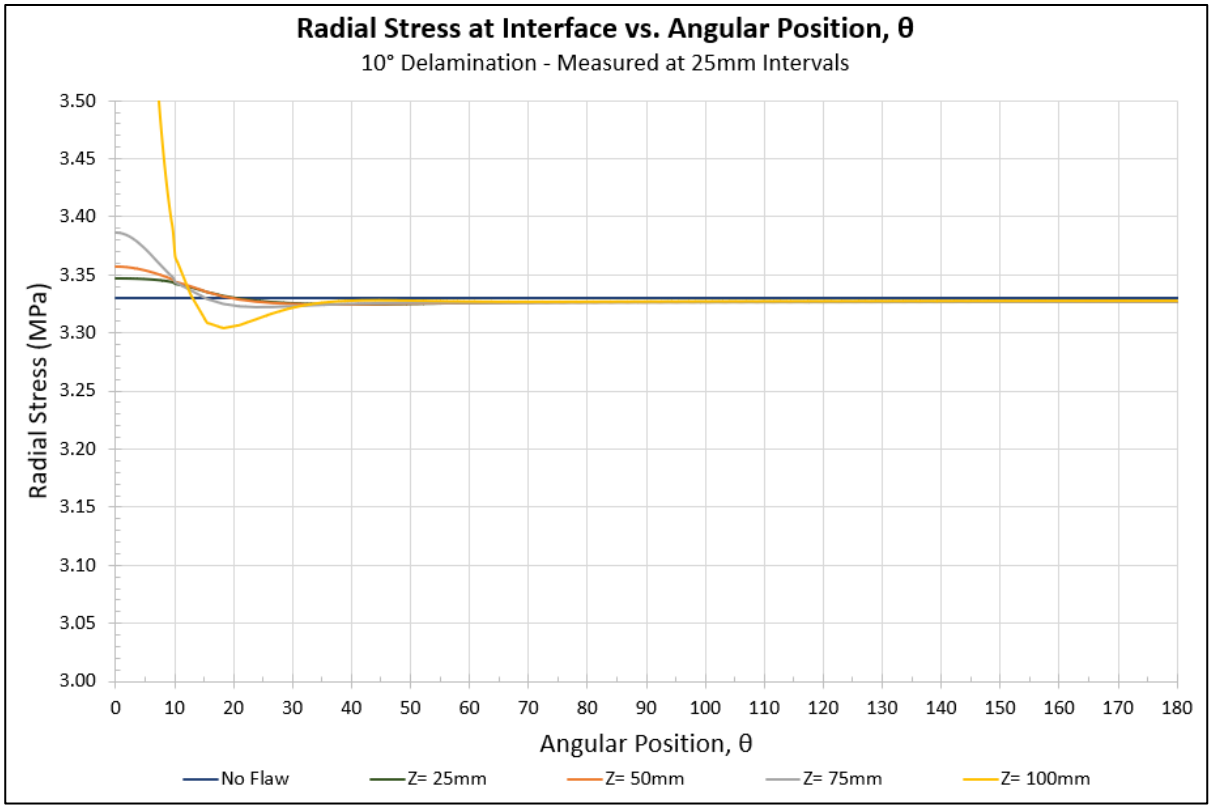

Figure 4.4b - Radial stress along propellant-insulation interface for 10° Delamination measured at 25mm intervals

4.3 Three-Dimensional Analysis Discussion

As shown three-dimensional stress analysis provided new insight on flaw induced stresses at the propellant-insulation interface. Stress trends at the delamination center line are identical to what is observed in the two-dimensional analysis confirming the assumption the two-dimensional simulations are representative of a stress analysis at the midplane of a flaw (See Section A-A in Figure 3.1). Moreover, three-dimensional analysis provided valuable insight on flaw-induced stress perturbations on a larger scale. This provides data key to developing a more holistic health diagnosis of SRMs than those discussed and critiqued in Chapter 1.5. However, the presented results are preliminary and can be improved in several ways. Such improvement can provide even more insightful data, increasing the effectiveness of a sensor based SRM structural diagnosis.

4.3.1 Three-Dimensional Stress Analysis Results and SRM Health Diagnosis

The provided three-dimensional stress analysis results shows there is much more to consider developing an effective health diagnosis method for SRMs. The most glaring observation is the unique radial stress plots associated with the delamination centerline and flaw tip planes. Though the plots produce expected trends considering what is understood from fracture and damage mechanic concepts, they are only observable at key locations, hence the need for a three-dimensional stress analysis. Additional radial stress readings show remnants of stress singularities from the delaminations exist outside of the planes of these key locations. Understanding of these trends are key to developing an improved sensor-based health diagnosis.

The results suggest that a sensor-based health diagnosis method will require more advanced DBST sensors at various lengths and angular positions pm an SRM. The chances of sensors being place in plane with a flaw is unlikely. Even if this occurs, the chance of the sensor being within 5° of the either circumferential flaw tip is even more unlikely. To address this, I propose a radially staggered multi-sensor array placed at a varying longitudinal interval. Having the sensors radially staggered ensures they measure radial stresses at as many places along the circumference of the propellant-insulation interface as possible. This increases the likelihood to detect remnants of stress singularities from flaws. As for the varying longitudinal intervals, I suggest placing the sensors at short intervals closer to the mid-span of the SRM and longer intervals near the ends. This is because flaws are more likely to nucleate at the midspan of the SRM than at the end due stress relieving flaps as noted in Chapter 3.1. Regarding the DBST sensors, they were most recently designed to have an accuracy of ±10 kPa or .01 MPa [9]. I believe the proposed

methodology is limited by this capacity. DBST sensors with an accuracy of ±1 kPa can detect stress perturbations from flaws more easily. At that scale, they can even detect the very slight reduction in radial stress seen in the 10° Delamination radial stress plots in Figure 4.4b.

4.3.2 Limitation to Three-Dimensional Stress Analysis

There are trends in the presented delamination radial stress plots that raise several questions. For example, in Chapter 4.2 it was assumed that delaminations at the propellant-insulation interface have no preference in which direction they propagate. However, the radial stress curves in Figure 4.4a suggest otherwise. If the aforementioned assumption is true, then equivalent peaks in stress would be observed at the circumferential flaw tip and the flaw tips at the X-Y plane. This is further illustrated in Figure 4.5 below. Here we see the

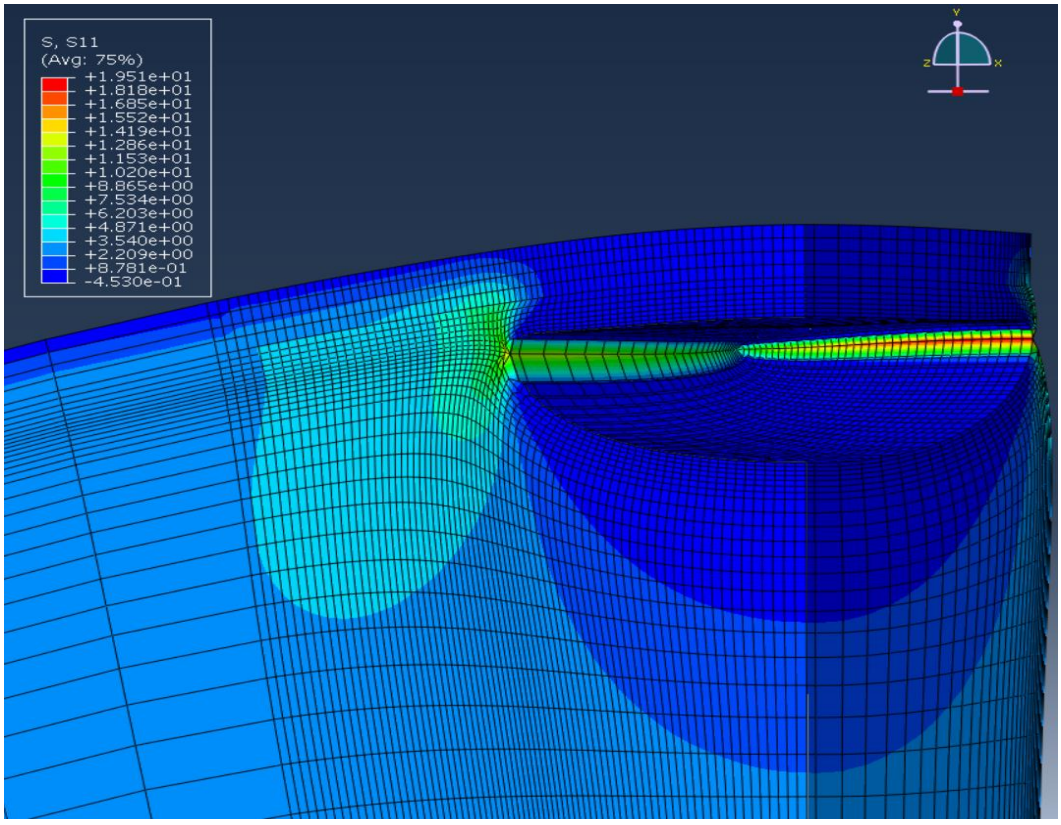

Figure 4.5 – Radial stress contour plot of three-dimensional 10° delamination after deformation

maximum stress at the circumferential flaw tip is around 13 MPa while the maximum radial stress at the flaw tips along the X-Y plane is 19 MPa. This suggest the delaminations will propagate more in the longitudinal direction than the circumferential direction, meaning the dimensions used may not be valid. To determine proper dimensions for the delamination will require further experimental investigation.

4.3.3 Suggested Improvements for Three-Dimensional Stress Analysis

My first suggested improvement to the current three-dimensional models is how the delaminations are modeled. Currently, models are modeled and simulated assuming the delamination is stationary. However, delaminations will likely propagate during the simulated cooling process. One way to implement this into the three-dimensional models Is by employing the virtual crack closure technique (VCCT). The VCCT was developed by Rybicki and Kanninen in 1977 to evaluate stress intensity factors in double cantilever beam samples using finite element calculations with modified crack closure integrals [22]. The technique assumes work required to close a crack is equivalent to the energy dissipated during crack growth. Benefits of using the VCCT method include its applicability to three-dimensional cracks and not requiring a high mesh density [24]. This makes the technique a great contender for more advance three-dimensional delamination models in the future.

Another advanced technique to consider for modeling delaminations is the cohesive zone model (CZM). The CZM was developed almost simultaneously by two independent researchers in the 1960's [25] [26]. Both researchers were attempting to physically describe the nonlinear processes that occur at the tip of a crack. The method assumes the presence of a cohesive zone in the direction the crack is propagating. In this cohesive zone, nonlinear traction-separation relations can be described with experimentally obtained

strain energy release rates [24]. This method is quite powerful and a popular method to analyze flaws in composite materials. Drawbacks to the method include dependence on high mesh density in the finite element model and necessity of experimentally obtained strain energy release rates.

Both the VCCT and CZM address inherit limitations of linear elastic fracture mechanics concepts. Implementation of either method would remove the necessity to directly model plastic zones for delaminations and even bore cracks moving forward. Both methods are also built into the FEM software Abaqus making them accessible. From my understanding of both methods, use of the VCCT for delaminations and CZM for bore cracks is a good start to improving my three-dimensional stress analysis moving forward.

An additional improvement to consider for my three-dimensional analysis is implementation of a nonlinear viscoelastic material response for the solid propellant. Though it is suggested that a thermal-elastic material response is sufficient for my preliminary analysis, determining if use of nonlinear viscoelastic material parameters effects my results is worth experimental investigation. Doing so in conjunction with more advanced flaw modeling methods can provide more insight on flaw-induced stress perturbation patterns in SRMs. More specifically, how flaws and their associated stresses propagate through a SRMs both circumferentially and longitudinally.

5. Conclusions and Future Work

5.1 Conclusions

The large amounts of capital invested in SRMs and the high stakes of the missions they support are reasons why an effective structural diagnosis is important. Existing methodologies to monitor the health of SRMs vary from use of strain monitoring polymer optical fibers to monitoring electrical-mechanical impedance spectra of piezoelectric sensors near flaws. A sensor and stress analysis-based methodology developed by research collaborators at the Edwards, CA Air Force Research Laboratory is also discussed, and its limitations addressed. These limitations being stress analysis is only conducted for two-dimensional SRM models and the simplified approach to modeling the flaws. I proposed that a three-dimensional finite element stress analysis of flawed SRMs models can provide more insightful data for a more effective structural diagnosis technique.

This thesis specifically details the stress analysis and how it can be used to develop such a structural health monitoring technique. Finite element modeling software Abaqus is used to simulate the post-cure cooling of SRMs in storage and analyze stresses that occur during this process. SRM models without flaws were simulated to determine baseline radial stress values that occur in undamaged rockets. Bore cracks and delaminations were added to two-dimensional models and simulated to observe stress effects from the flaws. It was found that flaw-induced stress perturbations can be observed at a SRMs solid propellant-insulation interface. These stress perturbations are unique to each flaw type, size, and location.

Then delaminations were added to three-dimensional models and simulated under the same conditions. Radial stress measured at the propellant-insulation interface at the

center line of the delamination produced identical trends to the two-dimensional stress analysis results. This validates the assumption that the two-dimensional models presented represent stress analysis at the midplane of a flaw. Remnants of stress concentrations from the delamination flaw tips can be observed longitudinally across a SRM as well. The distance at which such remnants can be observed is dependent on the size of the delamination. In both the two-dimensional and three-dimensional models, reduction in radial stresses were observed when compared to the baseline undamaged models. This suggest reductions in radial stress readings measured by DBST sensors located at the propellant-insulation interface can be indicative of the presence of a flaw. All of the observed patterns can serve as the foundation of a DBST sensor-based structural diagnosis technique for SHMs.

The three-dimensional stress analysis suggest it may be difficult to detect the location of delaminations using DBST sensors due to the small window at which stress perturbations from them exist. Due to this, I proposed a radially staggered multi-sensor array spaced at varying longitudinal intervals. Such a configuration measures radial stresses at more points along the circumference of the solid propellant-interface, increasing the chance it measures a flaw-induced stress perturbation. This in turn may allow for the prediction of size and location of the associated delaminations.

5.2 Future Work

As discussed in Chapter 3.3 and 4.3 there are several ways the three-dimensional finite element models can be improved. The improvements include using more advance crack modeling methods such as the virtual crack closure technique and cohesive zone model. Such methods will also prove beneficial when bore cracks are introduced the three-

dimensional finite element models. Another improvement to the models will be inclusion of nonlinear viscoelastic material parameters for the solid propellant in place of the thermal-elastic material parameter used. Implementation of the described improvements allows for a more accurate analysis of flaw induced stresses which in turn produces a more effective structural diagnosis technique.

Even with such improvements, the presented methodology is just the beginning of a much more holistic structural diagnosis technique for SRMs. In the future, I plan to incorporate physics informed neural networks trained by three-dimensional stress analysis data. Doing so would allow for the design of a neural network capable of detecting flaw type, size, and location in a SRM by reviewing unlabeled DBST sensor readings. Furthermore, such a neural network can monitor DBST sensor readings to predict the nucleation and propagation of flaws as well. This proposed structural health prognosis and diagnosis of SRMs is holistic, effective, and possibly the future of structural health monitoring techniques.

References

[1] S. Chaturvedi and P. Dave, "Solid propellants: AP/HTPB composite propellants," *Arabian Journal of Chemisty,* vol. 12, no. 8, pp. 2061-2068, 2019.

[2] T. Sojourner et al, "Solid Rocket Booster Reliability and Historical Failure Modes Review," in *51st AIAA/SAE/ASEE Joint Propulsion Conference*, Orlando, Fl, 2015.

[3] M. Walid, "Service life prediction of AP/Al/HTPB solid rocket propellant with consideration of softening aging behavior," *Chinese Journal of Aeronautics,* vol. 32, no. 2, pp. 361-368, 2019.

[4] G. Tussiwand et al, "Fracture mechanics of composite solid rocket propellant grains: Material testing," *Journal of Propulsion and Power,* vol. 25, no. 1, pp. 60-73, 2009.

[5] R. Frederick, B. Williams and S. Farmer, "Predicting and analyzing X-rays to measure propellant crack propagation speed," *Journal of Propulsion and Power,* vol. 12, no. 2, pp. 310-318, 1996.

[6] California Science Center , "Space Shuttle Endeavour," [Online]. Available: https://californiasciencecenter.org/exhibits/endeavour-experience/space-shuttle-endeavour. [Accessed 1 May 2021].

[7] W. A. Choy, "Structural Health Monitoring with Deep Learning," in *International MultiConference of Engineers and Computer Scientists*, Hong Kong, 2018.

[8] H. Chelner and J. Buswell, "Embeddable Structural Sensors for SHM of Solid Rocket Motor Grains," in *Defense and Security Symposium*, Orlando, Fl, 2006.

[9] A. Le et al, "Health Monitoring and Diagnosis of Solid Rocket Motors with Bore Cracks," *Journal of Aerospace Engineering,* vol. 29, no. 3, 2016.

[10] A. Le et al, "Detectability of Delaminations in Solid Rocket Motors with Embedded Stress Sensors," *Journal of Propulsion and Power,* vol. 29, no. 2, pp. 299-304, 2013.

[11] C. Riziotis et al, "Polymer Fiber Optic Sensors for Strain Monitoring in Solid Rocket Motors' Propellant," in *2013 Conference on Lasers and Electro-Optics*, 2013.

[12] C. Riziotis et al, "Fiber Optic Architectures for Strain Monitoring of Solid Rocket Motors' Propellant," *Sensor Letters,* vol. 11, pp. 1403-1407, 2013.

[13] L. Xiao et al, "Investigation of piezoelectric impedance-based health monitoring of structure interface debonding," in *SPIE Smart Structures and Materials + Nondestructive Evaluation andHealth Monitoring*, Las Vegas, NV, 2016.

[14] Y. Kamm and A. Gany, "Solid Rocket Motor Optimization," in *44th AIAA/ASME/SAE/ASEE Joint Propulsion Conference & Exhibit*, Hartford, CT, 2008.

[15] J. Delmonte, "Technology of Carbon and Graphite Fiber Composites", New York: Krieger Pub Co, 1987.

[16] D. Li, *Elastography mapping and microstructural analysis of heterogeneous materials,* Irvine, CA: University of California, Irvine, 2020.

[17] G. Irwin, "Analysis of Stresses and Strains Near the End of a Crack Traversing a Plate," *Journal of Applied Mechanics,* vol. 24, pp. 361-364, 1957.

[18] R. John et al, "Crack Growth Induced by Thermal-mechanical Loading," *Experimental Mechanics,* vol. 32, pp. 102-108, 1992.

[19] X. Tong et al, "A nonlinear viscoelastic constitutive model for cyclically loaded solid composite propellant," *International Journal of Solids and Structures,* vol. 198, no. 1, pp. 126-135, 2020.

[20] T. Birkan and Ö. Şebnem, "Constitutive modeling of solid propellants for three dimensional nonlinear finite element analysis," *Aerospace Science and Technology,* vol. 69, pp. 290-297, 2017.

[21] N. Perez, "Crack Tip Plasticity," in *Fracture Mechanics*, Academic Press, 2012.

[22] E. Rybicki and M. Kanninen, "A finite element calculation of stress intensity factors by a modified crack closure integral," *Engineering Fracture Mechanics,* vol. 9, no. 4, pp. 931-938, 1977.

[23] J. Reiner and R. Vaziri, "8.4 Structural Analysis of Composites With Finite Element Codes: An Overview of Commonly Used Computational Methods," in *Comprehensive Composite Materials II*, Elsevier, 2018, pp. 61-84.

[24] D. Dugdale, "Yielding of steel sheets containing slits," *Journal of the Mechanics and Physics of Solids,* vol. 8, no. 2, pp. 100-104, 1960.

[25] G. Barenblatt, "The mathematical theory of equilibrium cracks in brittle fracture," *Advances in Applied Mechanics,* vol. 7, pp. 55-129, 1962.

[26] A. Ted, *Fracture Mechanics: Fundamentals and Applications*, Third Edition, Boca Raton, FL: CRC PRess, 2005.

[27] K. George et al "Recent developments in elastomeric heat shielding materials for solid rocket motor casing application for future perspective," *Polymer Advanced Technologies,* vol. 29, no. 8, pp. 8-21, 2018.

[28] Northrop Grumman, "GEM 63XL QM-1 Static Test," Northrop Grumman Co, Falls Church, VA, 2020.

[29] D. Broek, "The crack tip plastic zone," in *Elementary engineering fracture mechanics*, Springer, 1982.